Stopped-Flow and Steady-State Study of the Diphenolase Activity of Mushroom Tyrosinase†

José Neptuno Rodríguez-López,‡ Lorena G. Fenoll,‡ Pedro Antonio García-Ruiz,§ Ramón Varón,|| José Tudela,‡ Roger N. F. Thorneley,⊥ and Francisco García-Cánovas*,‡

Grupo de Investigación de Enzimología, Departamento de Bioquímica y Biología Molecular A, Facultad de Biología, Departamento de Química Orgánica, Facultad de Química, Universidad de Murcia, E-30100 Espinardo, Murcia, Spain, Departamento de Química-Física, Escuela Técnica Superior de Albacete, Universidad de Castilla−La Mancha, E-02071, Albacte, Spain, and Department of Biological Chemistry, John Innes Centre, NR4 7UH Norwich, United Kingdom

Received March 8, 2000; Revised Manuscript Received May 18, 2000

ABSTRACT: The reaction of mushroom (*Agaricus bisporus)* tyrosinase with dioxygen in the presence of several *o*-diphenolic substrates has been studied by steady-state and transient-phase kinetics in order to elucidate the rate-limiting step and to provide new insights into the mechanism of oxidation of these substrates. A kinetic analysis has allowed for the first time the determination of individual rate constants for several of the partial reactions that comprise the catalytic cycle. Mushroom tyrosinase rapidly reacts with dioxygen with a second-order rate constant $k_{+8} = 2.3 \times 10^7$ M^{-1} s^{-1}, which is similar to that reported for hemocyanins [$(1.3 \times 10^6)-(5.7 \times 10^7)$ M^{-1} s^{-1}]. Deoxytyrosinase binds dioxygen reversibly at the binuclear Cu(I) site with a dissociation constant $K_D^{O_2} = 46.6$ μM, which is similar to the value ($K_D^{O_2} =$ 90 μM) reported for the binding of dioxygen to *Octopus vulgaris* deoxyhemocyanin [Salvato et al. (1998) *Biochemistry 37,* 14065−14077]. Transient and steady-state kinetics showed that *o*-diphenols such as 4-*tert*-butylcatechol react significantly faster with mettyrosinase ($k_{+2} = 9.02 \times 10^6$ M^{-1} s^{-1}) than with oxytyrosinase ($k_{+6} = 5.4 \times 10^5$ M^{-1} s^{-1}). This difference is interpreted in terms of differential steric and polar effects that modulate the access of *o*-diphenols to the active site for these two forms of the enzyme. The values of k_{cat} for several *o*-diphenols are also consistent with steric and polar factors controlling the mobility, orientation, and thence the reactivity of substrates at the active site of tyrosinase.

Tyrosinase (monophenol, *o*-diphenol:oxygen oxidoreductase, EC 1.14.18.1) is a copper-containing enzyme that is widely distributed throughout microorganisms, plants, and animals. It is of central importance in such processes as vertebrate pigmentation and the browning of fruits and vegetables (*1*, *2*). However, tyrosinases isolated from several different sources have similar structural and functional characteristics (*3*). Tyrosinases catalyze the *o*-hydroxylation of monophenols (monophenolase reaction) and the oxidation by molecular oxygen of *o*-diphenols to *o*-quinones (diphenolase reaction) (*4*−*6*). The catalytic cycles for the monophenolase and diphenolase activities are coupled not only to each other but also to nonenzymic reactions involving the *o*-quinone products (*7*, *8*).

Mushroom (*Agaricus bisporus*) tyrosinase (M_r 11.2×10^4) comprises two H subunits (M_r 4.3×10^4) and two L subunits (M_r 1.3×10^4) and contains two binuclear copper sites per tetramer (*9*). The copper, which is essential for the enzymatic activity, is present as "type 3" Cu(II) in the resting enzyme but is electron paramagnetic resonance (EPR) undetectable (*10*), suggesting antiferromagnetic spin coupling between the two Cu(II) ions in each center (*11*). Type 3 Cu(II) centers are ubiquitous, being present in proteins with diverse biological functions such as hemocyanin, laccase, ceruloplasmin, and ascorbate oxidase (*12*, *13*). Met, deoxy, and oxy forms of tyrosinase have been identified during the catalytic cycle (*5*, *14*, *15*). Oxytyrosinase has electronic and vibrational spectral features which are very similar to those of oxyhemocyanin, the oxygen transport protein found in some molluscs and arthropods (*16*). The structure of oxyhemocyanin from the arthropod *Limulus polyphemus* has been determined by X-ray diffraction (*17*). The oxygen is coordinated to the binuclear site in a side-on (μ-η^2:η^2) peroxide geometry, as first reported for a model compound (*18*). The relationship of this structure to the spectroscopic characteristics of oxytyrosinase and the reactivity of the coordinated peroxide have been discussed by Baldwin et al. (*19*) and Solomon et al. (*20*).

Ingraham (*21*) showed that the K_m for O_2 for French-prune tyrosinase depends on the structure of the *o*-diphenol hydrogen donor. A similar variation in the K_m for O_2 was observed by Duckworth and Coleman (*22*) working with mushroom tyrosinase. Several reaction mechanism have been proposed to explain this dependence (*21*−*23*); however, none

† This work was supported in part by a grant from the Ministerio de Educación y Cultura (Spain), Project PB98-0403-C02, and from the EU Human Capital and Mobility Program "Peroxidases in Agriculture, the Environment and Industry" (Contract ERB FMRX-CT98-0200). J.N.R.-L. thanks the Fundación Séneca (Murcia, Spain) for financial support at the John Innes Centre (Norwich, U.K.) for the project entitle "Structure-function relationship of mushroom tyrosinase". L.G.F. has a fellowship from Fundación Séneca (Murcia, Spain).

* To whom correspondence should be addressed: fax 00-34-968-363963 or 00-34-968-364147; e-mail canovasf@fcu.um.es.

‡ Facultad de Biología, Universidad de Murcia.

§ Facultad de Química, Universidad de Murcia.

|| Universidad de Castilla−La Mancha.

⊥ John Innes Centre.

10.1021/bi000539+ CCC: $19.00
Published on Web 08/03/2000

Scheme 1: Kinetic Reaction Mechanism for the Diphenolase Activity of Mushroom Tyrosinase[a]

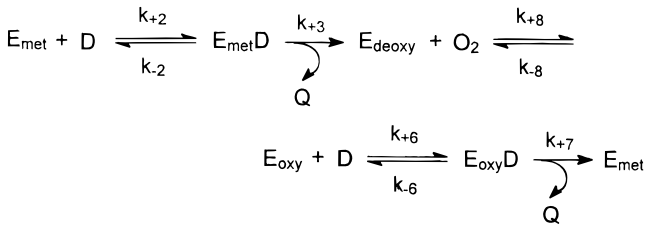

[a] Abbreviations: D, *o*-diphenol; Q, *o*-quinone; E_{met}, mettyrosinase or oxidized form of tyrosinase with $Cu^{2+}Cu^{2+}$ in the active site; E_{deoxy}, deoxytyrosinase or reduced form of tyrosinase with $Cu^{+}Cu^{+}$ in the active site; E_{oxy}, oxytyrosinase or oxidized form of tyrosinase with peroxide. The numeric notation of the rate constants is an extension of that previously used in Rodríguez-López et al. (*8*).

of these studies took into consideration the presence of three forms of tyrosinase (oxy, deoxy, and met). We have previously proposed a mechanism for mushroom tyrosinase (*8*, *24*) in which *o*-diphenol binds to the met and oxy forms but not to the deoxy form. Oxygen can only bind to the free deoxy form, which does not bind *o*-diphenol (Scheme 1). Although there have been several detailed steady-state kinetic investigations of tyrosinase (e.g. refs *8* and *22*), there have been few transient kinetic studies. In early studies, the reactivity of tyrosinase toward L-dopa and monophenolic substrates was investigated by stopped-flow spectrophotometry (*25*, *26*). However, there are to our knowledge no recent transient kinetic data on the reaction of tyrosinase with *o*-diphenols. The paucity of stopped-flow experiments with this enzyme is probably related to technical difficulties in data acquisition and analysis. Only small changes in the UV/visible absorption spectrum occur when the enzyme is mixed with oxygen or with oxidizable substrates. Moreover, the oxidation of substrates often yields highly colored products, which interfere with the small changes due to the type 3 copper centers.

In the present paper we report a detailed transient kinetic analysis for tyrosinase using the reaction sequence shown in Scheme 1. This has allowed us to calculate the second-order rate constants for the reaction of mettyrosinase with *o*-diphenols. The ability of ascorbic acid in the reaction medium to rapidly reduce the *o*-quinone products has been exploited to allow the measurement of the small absorption changes associated with the interconversion of tyrosinase transient species. Ascorbate also provides a convenient method for maintaining pseudo-first-order conditions at low substrate concentrations. In addition, we show how a method originally developed to determine rate constants for rapid peroxidase catalyzed reactions (*27*) can be usefully applied to the study of tyrosinase.

MATERIALS AND METHODS

Reagents. Mushroom tyrosinase (3300 units/mg), L-dopa, dopamine hydrochloride, 4-methylcatecol, L-dopa methyl ester and L-α-methyldopa were purchased from Sigma (Madrid, Spain), pyrogallol and 4-*tert*-butylcatechol were from Aldrich (Madrid, Spain), and catechol was from Fluka (Madrid, Spain). L-Ascorbic acid was obtained from Sigma and its concentration was determined by the lag period induced in the diphenolase activity of tyrosinase with L-dopa as substrate (*28*). Stock solutions of reducing substrates were prepared in 0.15 mM phosphoric acid in order to prevent autoxidation. All other chemicals were of analytical grade and supplied by Merck (Germany). Milli-Q system (Millipore Corp.) ultrapure water was used throughout this research.

Purification of Enzyme. Commercial mushroom tyrosinase was purified by the procedure of Duckworth and Coleman (*22*) but with two additional chromatographic steps. Enzyme solution was passed through a column (2.0 × 30 cm) of Sephadex G-100 (Pharmacia) equilibrated on 0.01 M sodium phosphate, pH 7.0. Samples showing tyrosinase activity were further purified by FPLC anion-exchange chromatography on a Mono-Q HR 5/5 column (Pharmacia) equilibrated with 0.01 M sodium phosphate buffer (pH 7.0) and eluted with sodium chloride (0−0.5 M gradient). Purified enzyme was desalted with Sephadex G-25 (Pharmacia) into ultrapure water and stored in liquid nitrogen. Tyrosinase concentration was determined by measuring the copper content of intact protein samples. Total enzyme copper was determined by atomic absorption analysis (external contract, Southern Science, Sussex, U.K.) with a diluted reference copper solution as a standard. Protein concentrations were determined by the method of Bradford (*29*) with bovine serum albumin as a standard.

Polarographic Assays. O_2 evolution was measured with a Hansatech DW oxymeter comprising a Teflon membrane-covered Clark-type electrode together with an Amel 863 digital X/Y recorder. The electrode was calibrated by the 4-*tert*-butylcatechol/tyrosinase method (*30*). The chamber of the polarograph (3.0 mL) contained 10 mM sodium phosphate buffer, pH 7.0, as the assay medium. Assays were carried out in the presence of a 5-fold excess of ascorbic acid over reducing substrate to avoid oxygen consumption by non-enzymatic reactions coupled to further oxidation of the *o*-quinone products. Different O_2 concentrations were obtained by mixing saturated aerobic and O_2-free solutions. O_2-free solutions were prepared by sparging with nitrogen gas. Thermostating at 25 °C was with a Haake D1G circulating water bath fitted with a heater/cooler and checked with a Cole-Parmer digital thermometer with a precision of ±0.1 °C.

Spectrophotometric Assays. Ultraviolet/visible absorption spectra of oxytyrosinase were recorded in quartz cuvettes (1 cm) on a Shimadzu UV-2101PC spectrophotometer with a spectral bandwidth of 1 nm at a scan speed of 120 nm/min. Oxytyrosinase concentrations were determined at 345 nm ($\epsilon = 18\ mM^{-1}\ cm^{-1}$). The assay medium was as used for polarographic assays. Reference cuvettes contained all the components except the substrate in a final volume of 1.0 mL.

Pre-Steady-State Kinetics. Absorbance changes of oxytyrosinase in the presence of different concentrations of 4-*tert*-butylcatechol were monitored in a stopped-flow spectrophotometer (model SF-51, Hi Tech Scientific, Salisbury, U.K.). Data were recorded through an RS232 interface with a microcomputer. The wavelength was set at 345 nm, the maximum for the absorption spectrum of oxytyrosinase. Oxytyrosinase reactions with 4-*tert*-butylcatechol were carried out in the presence of a 10-fold molar excess of ascorbic acid over reducing substrate. The reduction of the radical products by the excess ascorbate ensured a constant substrate concentration (pseudo-first-order conditions), as well as preventing the formation of colored products such as 4-*tert*-butyl-*o*-benzoquinone (*27*). Temperature was controlled at

25 °C in a Techne C-400 circulating bath with a heater/cooler. Maximal oxytyrosinase formation was achieved by adding hydroxylamine in 3-fold molar excess over the copper content of the enzyme (*31*).

Kinetic Data Analysis. Pre-steady-state kinetic data were analyzed by fitting the absorbance−time curves to exponential functions with a least-squares minimization program supplied by Hi Tech Scientific Ltd. To determine the kinetic constants for *o*-diphenols and oxygen, two different procedures and analyses were used, depending on the nature of the reducing substrates. The Michaelis constant of tyrosinase for oxygen ($K_m^{O_2}$) depends of the chemical nature of the *o*-diphenol reducing substrate (*21*). An initial rate method was used to determine steady-state kinetic constants for dopamine, catechol, 4-*tert*-butylcatechol, pyrogallol, and 4-methylcatechol oxidation at various concentrations of oxygen from triplicate polarographic measurements of v_0. Primary plots of $1/v_0$ versus $1/[O_2]_0$, at different *o*-diphenol concentrations, gave straight lines according to eq 8. The kinetic constants were determined from the secondary plots of the slope and *y*-axis intercept versus $1/[D]_0$ (eqs 13 and 14, respectively). However, an integrated rate equation method had to be used for substrates with a very low $K_m^{O_2}$ value (i.e. L-dopa, L-dopa methyl ester, and L-α-methyldopa). The values of V_{max}^{app} (the apparent maximum steady-state rate) and K_m^{app,O_2} (apparent Michaelis constant of tyrosinase toward oxygen) at different concentrations of *o*-diphenol were determined from the curvature evident in plots of oxygen consumption versus time (10 determinations). A constant concentration of *o*-diphenol was maintained during each time course by adding a 5-fold excess of ascorbic acid to the assay medium. Data were fitted by nonlinear regression to the integrated form (*32*) of the Michaelis equation (eq 18). The dependence of V_{max}^{app} and K_m^{app,O_2} versus $[D]_0$ was fitted by nonlinear regression to eqs 16 and 17, respectively, and the absolute kinetic constants calculated. The fitting was performed by using Marquart's algorithm (*33*) implemented in the SigmaPlot 2.01 program for Windows (*34*).

Kinetic Simulations. The kinetics of the reaction mechanism described in Scheme 1 is defined by a set of differential equations, whose numerical integration was carried out with a computer program designed by García-Sevilla et al. (*35*). Experimentally determined values of the equilibrium and rate constants were assigned to the partial reactions defined in Scheme 1.

RESULTS

Steady-state Kinetics

Kinetic Analysis. Mushroom tyrosinase is known to exhibit wide substrate specificity and to oxidize a number of *o*-diphenolic compounds. The enzyme requires one molecule of oxygen to oxidize two molecules of *o*-diphenol to two molecules of *o*-quinone. The diphenolase mechanism of tyrosinase is a linear system (Scheme 1) involving several rate constants. By applying a steady-state approach to Scheme 1, an analytical expression for the initial rate of oxygen consumption can be obtained:

$$v_0 = \frac{\alpha_1[D]_0[O_2]_0[E]_0}{\beta_0 + \beta_1[D]_0 + \beta_2[O_2]_0 + \beta_3[D]_0[O_2]_0} \quad (1)$$

where the coefficients α_1 and $\beta_0-\beta_3$ are

$$\alpha_1 = k_{+2}k_{+3}k_{+6}k_{+7}k_{+8}$$

$$\beta_0 = k_{+2}k_{+3}k_{-8}(k_{-6} + k_{+7})$$

$$\beta_1 = k_{+2}k_{+3}k_{+6}k_{+7}$$

$$\beta_2 = k_{+8}[k_{+2}k_{+3}(k_{-6} + k_{+7}) + k_{+6}k_{+7}(k_{-2} + k_{+3})]$$

$$\beta_3 = k_{+2}k_{+6}k_{+8}(k_{+3} + k_{+7}) \quad (2)$$

Equation 1 can be rewritten as

$$v_0 = \frac{V_{max}[D]_0[O_2]_0}{W + K_m^{O_2}[D]_0 + K_m^{D}[O_2]_0 + [D]_0[O_2]_0} \quad (3)$$

An earlier steady-state kinetic study of tyrosinases from different biological sources indicates the absence of fast pre-equilibria for the binding of *o*-diphenols to the met and oxy forms of these enzymes (*36*). Therefore, assuming that $k_{+3} \gg k_{-2}$ and $k_{+7} \gg k_{-6}$, the analytical expressions for V_{max} (maximum steady-state rate), W (concentration-independent term), $K_m^{O_2}$ (Michaelis constant of tyrosinase toward oxygen), and K_m^{D} (Michaelis constant of tyrosinase toward *o*-diphenol) are

$$V_{max} = \alpha_1[E]_0/\beta_3 = k_{+3}k_{+7}[E]_0/(k_{+3} + k_7) = k_{cat}[E]_0 \quad (4)$$

$$W = \beta_0/\beta_3 = k_{+3}k_{+7}k_{-8}/[k_{+6}k_{+8}(k_{+3} + k_{+7})] = k_{cat}K_D^{O_2}/k_{+6} \quad (5)$$

$$K_m^{O_2} = \beta_1/\beta_3 = k_{+3}k_{+7}/[k_{+8}(k_{+3} + k_{+7})] = k_{cat}/k_{+8} \quad (6)$$

$$K_m^{D} = \beta_2/\beta_3 = [k_{+3}k_{+7}(k_{+2} + k_{+6})]/[k_{+2}k_{+6}(k_{+3} + k_{+7})] = [k_{cat}(k_{+2} + k_{+6})]/k_{+2}k_{+6} \quad (7)$$

Determination of Tyrosinase Kinetic Constants by the Initial Rate Method. The $K_m^{O_2}$ with dopamine, catechol, 4-*tert*-butylcatechol, pyrogallol, and 4-methylcatechol as reducing substrates ranged from 20 to 60 μM (Table 1). An initial-rate method was used to determine the kinetic constants for these substrates. The initial rate of oxygen uptake exhibited a hyperbolic dependence on oxygen concentration at each *o*-diphenol concentration as predicted by eq 3 (data not shown). These data when plotted in a reciprocal form give a series of straight lines, which intersect to the left of the ordinate and above the abscissa axes when 4-*tert*-butylcatechol (Figure 1A), dopamine, catechol, and 4-methylcatechol were used as substrates of tyrosinase. However, with pyrogallol, the intersection was below the abscissa axis (Figure 1B). This dependence of the intersection point on the nature of the *o*-diphenolic substrate was also reported for apple tyrosinase by Janovitz-Klapp et al. (*23*).

The expression for the reciprocal plot of $1/v_0$ versus $1/[O_2]_0$ is

$$\frac{1}{v_0} = \left(\frac{W}{V_{max}}\frac{1}{[D]_0} + \frac{K_m^{O_2}}{V_{max}}\right)\frac{1}{[O_2]_0} + \frac{K_m^{D}}{V_{max}}\frac{1}{[D]_0} + \frac{1}{V_{max}} \quad (8)$$

Primary plots of $1/v_0$ versus $1/[O_2]_0$ predict a series of

Table 1: Kinetic Parameters and Rate Constants of Mushroom Tyrosinase for Several Phenolic Substrates

o-diphenol	(*x*,*y*)-intersect[a] (mM^{-1}, s mM^{-1})	$K_D^{O_2}$ (μM)	k_{cat} (s^{-1})	$K_m^{O_2}$ (μM)	K_m^{D} (mM)	k_{+6} (M^{-1} s^{-1})
pyrogallol	(−21.8, −145)	(46.0 ± 2.0)	(1263 ± 60)	(56.5 ± 4.3)	(2.16 ± 0.30)	(5.84 ± 1.0) × 10^5
catechol	(−21.2, 205)	(47.2 ± 2.1)	(878 ± 50)	(40.5 ± 4.0)	(0.10 ± 0.01)	(8.78 ± 1.2) × 10^6
4-methylcatechol	(−21.3, 253)	(47.0 ± 1.8)	(842 ± 25)	(35.8 ± 3.2)	(0.12 ± 0.021)	(7.02 ± 1.5) × 10^6
4-*tert*-butylcatechol	(−21.7, 626)	(46.1 ± 2.0)	(641 ± 20)	(28.0 ± 3.1)	(1.41 ± 0.20)	(4.55 ± 0.8) × 10^5
dopamine	(−21.0, 1345)	(47.7 ± 2.0)	(439 ± 25)	(21.5 ± 3.1)	(0.72 ± 0.10)	(6.10 ± 1.1) × 10^5
L-dopa		(46.7 ± 3.0)	(108 ± 9.1)	(6.5 ± 3.0)	(0.38 ± 0.04)	(2.82 ± 0.5) × 10^5
L-α-methyldopa		(45.0 ± 3.0)	(44.3 ± 4.2)	(2.2 ± 0.5)	(2.12 ± 0.19)	(2.10 ± 0.3) × 10^4
L-dopa methyl ester		(47.0 ± 3.0)	(35.5 ± 4.0)	(1.1 ± 0.3)	(0.91 ± 0.10)	(3.9 ± 0.6) × 10^4

[a] The (*x*,*y*)-intersects correspond to the intersection points of the straight lines from reciprocal plots at a concentration of 1 nM tyrosinase.

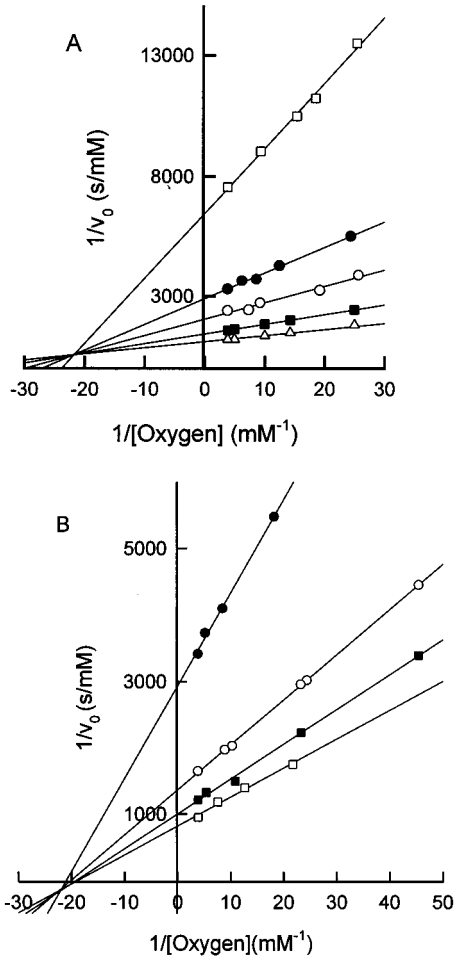

FIGURE 1: Lineweaver−Burk plots of the reaction of mushroom tyrosinase with *o*-diphenols and oxygen at pH 7.0 and 25 °C. (A) Effect of 4-*tert*-butylcatechol and oxygen concentration on the initial activity of tyrosinase (2.0 nM). The different 4-*tert*-butylcatechol concentrations were (□) 0.2, (●) 0.5, (○) 1.0, (■) 2.0, and (△) 3.0 mM. (B) Oxidation of pyrogallol with tyrosinase (1.5 nM). The pyrogallol concentrations were (●) 0.5, (○) 1.0, (■) 3.0, and (□) 5.0 mM. Each point represents the mean of five separate experiments.

convergent lines, the intersects of which have the following *x*,*y* coordinates:

$$x = -\frac{(k_{+2}+k_{+6})}{k_{+2}}\frac{k_{+8}}{k_{-8}} = -\frac{(k_{+2}+k_{+6})}{k_{+2}}\frac{1}{K_D^{O_2}} \quad (9)$$

$$y = \frac{1}{V_{max}}\left[1 - \frac{k_{cat}(k_{+2}+k_{+6})}{k_{-8}k_2}\right] \quad (10)$$

From these two equations, several interesting conclusions can be reached. The *x*-coordinate of the intercept (eq 9) is the product of two terms: the first includes the rate constants for the binding of *o*-diphenol to met- (k_{+2}) and oxytyrosinase (k_{+6}), and the second is the oxygen dissociation constant from free tyrosinase. Table 1 shows that the *x*-coordinate of the intercept is independent of the chemical nature of the *o*-diphenol with an average value of -21.4 mM^{-1}. This independence of the x-coordinate from the nature of the reducing substrate can be explained by assuming that $k_{+2} \gg k_{+6}$. Thus, eq 9 can be simplified to

$$x = -\frac{k_{+8}}{k_{-8}} = -\frac{1}{K_D^{O_2}} \quad (11)$$

The values of $K_D^{O_2}$ determined for the different *o*-diphenols are given in Table 1.

A positive or negative *y*-coordinate value for the intercept can be rationalized by considering eq 12, which is an alternative form of eq 10:

$$y = \frac{1}{V_{max}}\left(1 - \frac{k_{cat}}{k_{-8}}\right) = \frac{1}{[E]_0}\left(\frac{k_{-8}-k_{cat}}{k_{-8}k_{cat}}\right) \quad (12)$$

Thus, if $k_{cat} < k_{-8}$ a positive *y*-coordinate for the intercept results and with $k_{cat} > k_{-8}$ a negative coordinate, while if $k_{cat} = k_{-8}$ the intercept would lie on the abscissa with $y = 0$.

Secondary plots of the slope and *y*-axis ordinate obtained from the primary plots versus $1/[D]_0$ are described by eqs 13 and 14. The kinetic constants calculated from this analysis for all the *o*-diphenols used are given in Table 1.

$$\text{slope} = \frac{W}{V_{max}}\frac{1}{[D]_0} + \frac{K_m^{O_2}}{V_{max}} \quad (13)$$

$$y\text{ - axis} = \frac{K_m^{D}}{V_{max}}\frac{1}{[D]_0} + \frac{1}{V_{max}} \quad (14)$$

Determination of Kinetic Constants by an Integrated Rate Expression. When saturating concentrations of L-dopa, L-dopa methyl ester, or L-α-methyldopa (4, 10, and 20 mM, respectively) were oxidized in the presence of a high concentration of tyrosinase (0.2 μM), all the O_2 (0.26 mM) was consumed within the first seconds of the reaction. The time courses were linear for 70%, 82%, and 90% of oxygen consumption for L-dopa, L-α-methyldopa, or L-dopa methyl ester, respectively (data not shown) indicating a low $K_m^{O_2}$ value (<10 μM). Because of the low $K_m^{O_2}$ value for these substrates, the integrated Michaelis equation was used for the kinetic analysis. At a given concentration of *o*-diphenol,

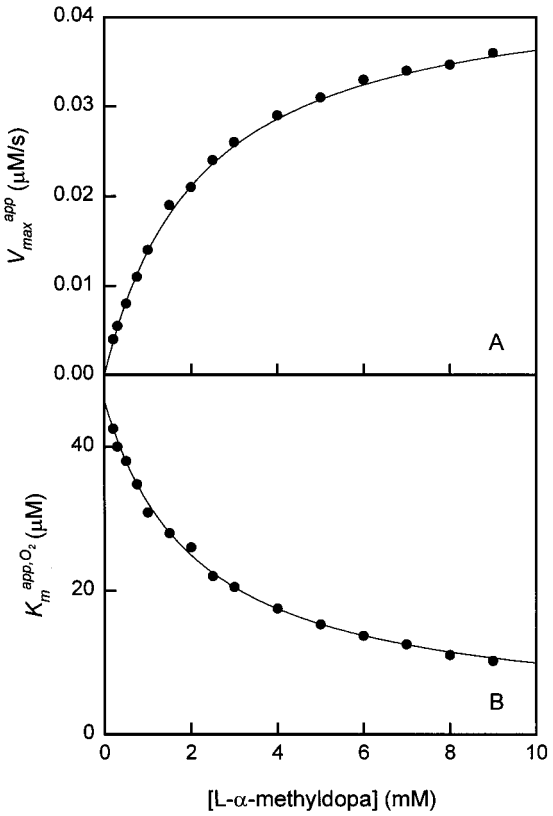

FIGURE 2: Dependence of (A) V_{max}^{app} and (B) K_m^{app,O_2} on the concentration of L-α-methyldopa for its oxidation by tyrosinase (1 nM) at pH 7.0 and 25 °C. Each point represents the mean of 10 separate experiments.

the Michaelis equation with respect to oxygen is

$$v_0 = \frac{V_{max}^{app}[O_2]_0}{K_m^{app,O_2} + [O_2]_0} \quad (15)$$

where the analytical expressions for V_{max}^{app} and K_m^{app,O_2} are given by

$$V_{max}^{app} = \frac{V_{max}[D]_0}{K_m^{D} + [D]_0} \quad (16)$$

$$K_m^{app,O_2} = \frac{W + K_m^{O_2}[D]_0}{K_m^{D} + [D]_0} \quad (17)$$

At a constant *o*-diphenol concentration (maintained by a 5-fold excess of ascorbic acid), eq 15 can be integrated between times 0 ($[O_2]_0$) and t ($[O_2]_t$) to yield

$$\frac{2.3}{t}\log\frac{[O_2]_0}{[O_2]_t} = -\frac{1}{K_m^{app,O_2}}\frac{[O_2]_0 - [O_2]_t}{t} + \frac{V_{max}^{app}}{K_m^{app,O_2}} \quad (18)$$

The values of V_{max}^{app} and K_m^{app,O_2} at different concentrations of *o*-diphenols were fitted by nonlinear regression to eqs 16 and 17, respectively (Figure 2), and the absolute values for V_{max} and $K_m^{O_2}$ were calculated (Table 1).

Determination of Elementary Rate Constants. From the kinetic constants listed in Table 1, several elementary rate constants can be calculated. Figure 3 shows a linear dependence of $K_m^{O_2}$ versus k_{cat}. According to eq 6, the inverse

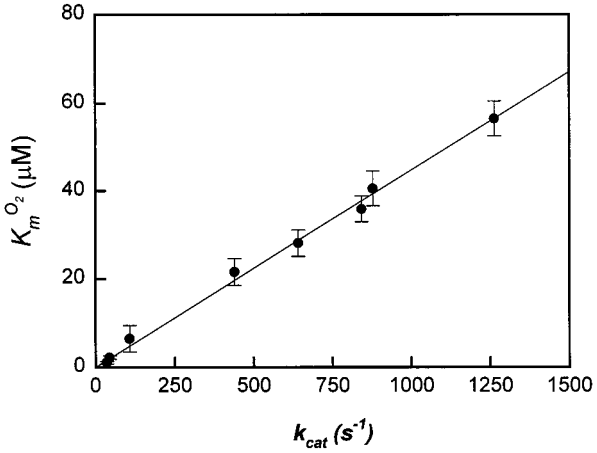

FIGURE 3: Dependence of $K_m^{O_2}$ on the k_{cat} values for different *o*-diphenolic substrates. Data are summarized in Table 1.

of the slope of this plot gives the value of the second-order rate constant for the binding of oxygen to E_{deoxy} [$k_{+8} = (2.3 \pm 0.4) \times 10^7$ M^{-1} s^{-1}]. $K_D^{O_2}$ was found to be independent of the nature of the *o*-diphenol (Table 1) with an average value of 46.6 ± 2.4 μM. This allows a value for $k_{-8} = (1.07 \pm 0.2) \times 10^3$ s^{-1} to be calculated. Pyrogallol is the only substrate with a k_{cat} value higher than k_{-8} (Table 1), which explains why the *y*-intercept of the series of lines obtained from the reciprocal plot has a negative value (eq 12). In addition, since we have deduced above that $k_{+2} \gg k_{+6}$, we can determine the value of the second-order rate constant for the binding of the *o*-diphenol to the E_{oxy} form of tyrosinase (k_{+6}). Thus, eq 7 can be simplified to

$$K_m^{D} = k_{cat}/k_{+6} \quad (19)$$

The values of k_{+6} for the different *o*-diphenols studied are listed in Table 1.

Transient-phase Kinetics

Kinetic Analysis. The kinetic mechanism for the reaction of oxytyrosinase with *o*-diphenols is shown in Scheme 1. The time course of the concentration of oxytyrosinase is given for

$$[E_{oxy}] = [E_{oxy}]_\infty + \sum_{h=1}^{4} A_h e^{-\lambda_h t} \quad (20)$$

where λ_1, λ_2, λ_3, and λ_4 are the square of the polynomial $\lambda^4 - G_1\lambda^3 + G_2\lambda^2 - G_3\lambda + G_4$ and the analytical expressions for $[E_{oxy}]_\infty$ and A_h are

$$[E_{oxy}]_\infty = \frac{g_4[E]_0}{G_4} \quad (21)$$

$$A_h = [E_0]\frac{\lambda_h^4 - g_1\lambda_h^3 + g_2\lambda_h^2 - g_3\lambda_h + g_4}{\lambda_h\prod_{\substack{p=1\\p\neq h}}^{4}(\lambda_h - \lambda_p)} \quad (h = 1-4) \quad (22)$$

The coefficients G_i ($i = 1-4$) and g_i ($i = 1-4$) are functions of the rate constants and of the initial concentrations of O_2

and *o*-diphenol. They are defined by the expressions shown in the Appendix.

Under the conditions used for the transient kinetic experiments at low $[D]_0$ (5−20 μM), the following relationship is fulfilled:

$$k_{+3}, k_{+7}, k_{+8}[O_2]_0, k_{-8} \gg k_{+2}[D]_0, k_{+6}[D]_0, k_{-2}, k_{-6}$$

and, moreover, k_{+3}, k_{+7}, $k_{+8}[O_2]_0$, and k_{-8} are of the some order of magnitude. Under these conditions eq 20 can be simplified to

$$[E_{oxy}] = [E_{oxy}]_\infty + A_1 e^{-\lambda_1 t} \quad (23)$$

where

$$[E_{oxy}]_\infty = \frac{k_{+2}[O_2]_0[E]_0}{k_{+2}K_D^{O_2} + (k_{+2} + k_{+6})[O_2]_0} \quad (24)$$

$$A_1 = \frac{(k_{+2}K_D^{O_2} + k_{+6}[O_2]_0)[E]_0}{k_{+2}K_D^{O_2} + (k_{+2} + k_{+6})[O_2]_0} \quad (25)$$

$$\lambda_1 = \frac{[k_{+2}K_D^{O_2} + (k_{+2} + k_{+6})[O_2]_0][D]_0}{K_D^{O_2} + [O_2]_0} \quad (26)$$

Reaction between Oxytyrosinase and 4-tert-Butylcatechol. Stopped-flow experiments are most easily performed and the data evaluated under pseudo-first-order conditions. Generally, a 10-fold excess of the substrate over the enzyme suffices. However, the use of substrate concentrations that ensure pseudo-first-order conditions can increase the rate of the reaction to beyond the stopped-flow range ($k_{obs} > 500$ s^{-1}). We have therefore used ascorbic acid to maintain a constant concentration of 4-*tert*-butylcatechol during reactions studied by stopped-flow spectrophotometry (*27*). Ascorbic acid reduces many radicals and *o*-quinones at high rates. When present with oxytyrosinase and 4-*tert*-butylcatechol, the *o*-quinone product is rapidly reduced to maintain a constant, steady-state concentration of substrate close to the initial concentration. Thus, pseudo-first-order conditions are maintained even though the concentration of the substrate may be very low. Moreover, ascorbic acid is also useful because it minimizes the accumulation of 4-*tert*-butyl-*o*-benzoquinone which has an intense absorption band in the visible region that compromises direct observation of the spectral changes associated with the copper centers of the tyrosinase.

Oxytyrosinase has a relatively intense band at 345 nm, and the time dependence of the absorbance changes at this wavelength (Figure 4) can be fitted to a simple exponential function (eq 23). Under pseudo-first-order conditions, a plot of λ_1 versus the concentration of 4-*tert*-butylcatechol was linear and passed through the origin (Figure 5). However, the term $[E_{oxy}]_\infty$ was independent of the concentration of 4-*tert*-butylcatechol (Figure 5). These dependencies can be explained by the kinetic analysis described above with eqs 26 and 24, respectively. $[E_{oxy}]_\infty$ had a value of 0.95 μM, which corresponded to 95% of the initial oxytyrosinase present in the assay ($[E_{oxy}]_0 = 1.0$ μM). Figure 6 shows two simulations of the change in E_{oxy} concentration with time based on Scheme 1, assuming $k_{+2} \gg k_{+6}$ (case A) and $k_{+2} \ll k_{+6}$ (case B). Since E_{oxy} is the only species absorbing at 345 nm, the small change in absorbance observed in these transient kinetic experiments means that $k_{+2} \gg k_{+6}$ ($[E_{oxy}]_\infty = 0.9514$ μM). Therefore eq 26 can be simplified to

$$\lambda_1 = k_{+2}[D]_0 \quad (27)$$

which explains the linear dependence of λ_1 on the concentration of 4-*tert*-butylcatechol passing through the origin (Figure 5). The slope of this straight line gives the second-order rate constant for the reaction of mettyrosinase with 4-*tert*-butylcatechol [$k_{+2} = (9.02 \pm 0.5) \times 10^6$ M^{-1} s^{-1}], which is approximately 20-fold higher than the value for the binding of this substrate to oxytyrosinase [$k_{+6} = (4.5 \pm 0.8) \times 10^5$ M^{-1} s^{-1}] (Table 1).

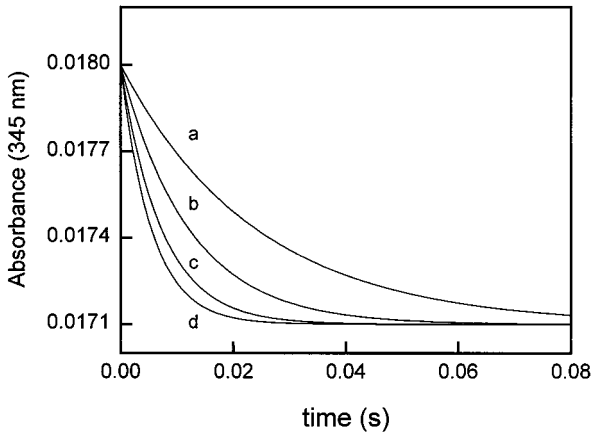

FIGURE 4: Stopped-flow time courses at 345 nm for the reaction of oxytyrosinase (1.0 μM) with 4-*tert*-butylcatechol in 10 mM phosphate buffer at pH 7.0 and 25 °C. Concentrations of 4-*tert*-butylcatechol concentrations were (a) 5, (b) 10, (c) 15, and (d) 20 μM. Each point represents the mean of 10 separate experiments.

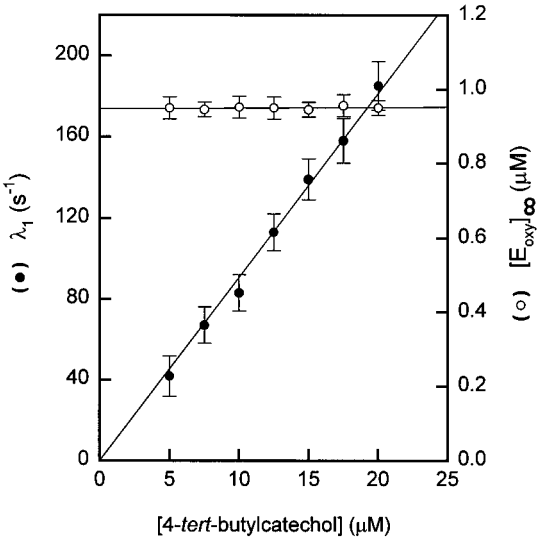

FIGURE 5: Dependence of apparent-first-order rate constant, λ_1, and $[E_{oxy}]_\infty$ for the reaction of mushroom tyrosinase with 4-*tert*-butylcatechol as a function of substrate concentration at pH 7.0.

DISCUSSION

Binding of o-Diphenols to Tyrosinase. The binding of *o*-diphenols to tyrosinase most likely involves several molecular processes that include diffusion to the active site and orientation of the substrate followed by coordination of a phenolic oxygen atom to one of the type 3 copper ions. Clearly such reactions may be facilitated or retarded by

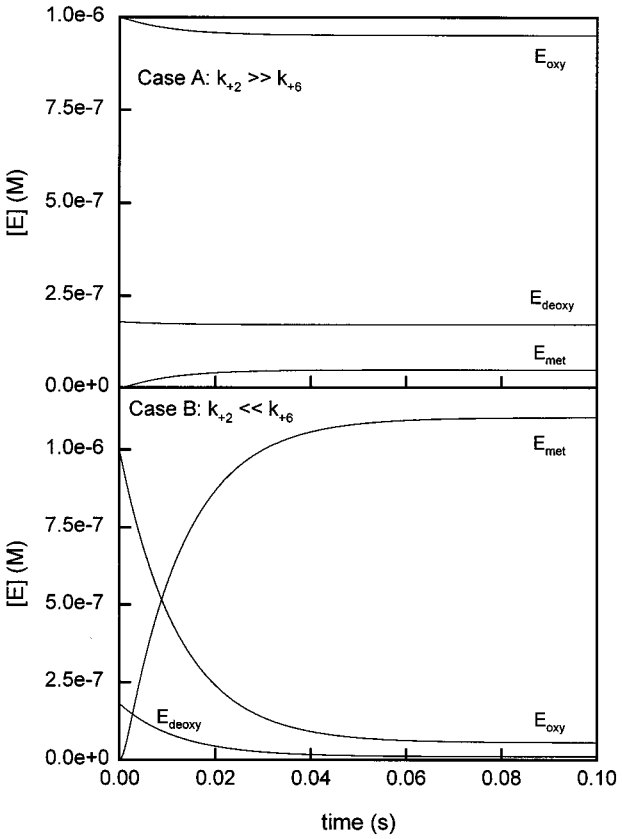

FIGURE 6: Simulation results of the reaction of tyrosinase with 4-*tert*-butylcatechol and oxygen according to Scheme 1. The initial concentrations of the enzymatic species were $[E_{met}]_0 = 0$, $[E_{deoxy}]_0 = 0.179$ μM, and $[E_{oxy}]_0 = 1.0$ μM. Initial concentration of E_{deoxy}, at 1.0 μM of E_{oxy}, was calculated according to the equilibrium. The experimentally calculated value of $K_D^{O_2} = 46.6$ μM was used for enzyme concentration calculations. The $[O_2]_0 = 0.26$ mM and $[D]_0 = 10$ μM were assumed constant throughout the simulated time course. For both cases illustrated in this figure, the following rate constants were used: $k_{-2} = 0.1$ s^{-1}, $k_{+3} = 10^3$ s^{-1}, $k_{-6} = 0.1$ s^{-1}, $k_{+7} = 10^3$ s^{-1}, $k_{+8} = 2.3 \times 10^7$ M^{-1} s^{-1} and $k_{-8} = 1.07 \times 10^3$ s^{-1}. The values for the second-order rate constants k_{+2} and k_{+6} were, for case A, $k_{+2} = 9.02 \times 10^6$ M^{-1} s^{-1} and $k_{+6} = 4.55 \times 10^5$ M^{-1} s^{-1}, and for case B, $k_{+2} = 4.55 \times 10^5$ M^{-1} s^{-1} and $k_{+6} = 9.02 \times 10^6$ M^{-1} s^{-1}.

Scheme 2: Proposed Structural Changes Occurring during the Reaction of Mettyrosinase with *o*-Diphenols[a]

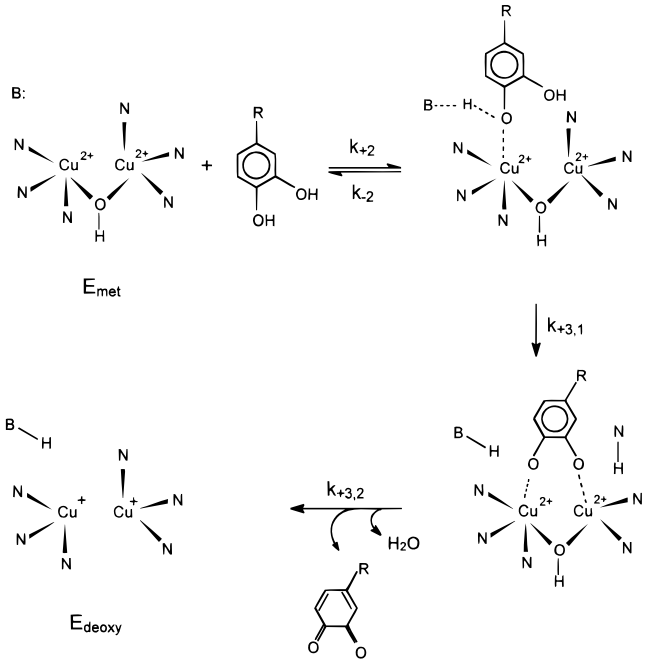

[a] This scheme is similar to the mechanism proposed by Solomon and Lowery (*45*) and reviewed in Solomon et al. (*20*), with the inclusion of a basic group (B) to catalyze proton transfer from the coordinating hydroxyl. The reaction designated k_{+3} has been separated into two substeps, $k_{+3,1}$ and $k_{+3,2}$, in order to aid the discussion of the rate-limiting step in the oxidation of *o*-diphenols by mushroom tyrosinase. The two copper ions of the binuclear site and the six histidines coordinated to the copper atoms are shown, but coordinated waters are omitted for clarity. In the diphenolase activity, the *o*-diphenol binds to the axial position of one of the coppers of the met site, perhaps Cu_A. Coordination of the *o*-diphenol is accompanied by proton transfer to a protein residue represented by B. Bidentate coordination of the *o*-diphenol is accompanied by a second proton transfer, probably by displacement of an axial histidine coordinated to Cu_B. Electron transfer from the catechol substrate results in the formation of the *o*-quinone and the deoxy form of the binuclear copper site. The value of $k_{+3,1}$ is proposed to be dependent on the size and polarity of the side chain of the *o*-diphenol substrate, thus explaining the variation in k_{cat}.

interactions with amino acid side chains present in the vicinity of the binuclear copper center (Schemes 2 and 3). Diffusion and orientation are most likely to involve steric factors while coordination to the copper is more likely to involve acid/base catalysis. Steric constraints on access of *o*-diphenols to the active site of oxytyrosinase are clearly shown by the range in the values of k_{+6} listed in Table 1. *o*-Diphenols with small substituent side chains (e.g., 4-methylcatechol, $k_{+6} = 7 \times 10^6$ M^{-1} s^{-1}) bind to oxytyrosinase at similar rates to catechol ($k_{+6} = 9 \times 10^6$ M^{-1} s^{-1}), which has no substituent side chain. The absence of steric hindrance on these substrates binding is reflected in a second-order rate constant close to 10^7 M^{-1} s^{-1}, which is typical for small molecules binding to "relatively open" active sites in proteins [e.g., oxygen binding to both tyrosinase and hemocyanin (see below)]. *o*-Diphenols with larger and/or charged side chains bind up to 200-fold slower than catechol (e.g., L-dopa methyl ester, $k_{+6} = 3.9 \times 10^4$ M^{-1} s^{-1}, Table 1). Although the trihydroxylated compound pyrogallol has no side chain, the presence of an additional hydroxyl group causes it to bind to oxytyrosinase with a 15-fold lower rate constant than catechol (Table 1). This may also be a steric effect of the additional hydroxyl group in pyrogallol or reflect the difference in pK_a of the hydroxyl that is proposed to coordinate to the copper.

The steady-state and transient kinetic data show that *o*-diphenols bind much faster to met- than to oxytyrosinase ($k_{+2} \gg k_{+6}$). In the absence of a three-dimensional structure for any tyrosinase in either state, explanations in terms of protein conformation changes must be highly speculative. However, a related enzyme, potato catechol oxidase, showed no significant conformational changes between reduced and oxidized states (*37*). Most of the mechanisms proposed to describe the binding of *o*-diphenols to tyrosinase involve the initial coordination of the reducing substrate to one of the two copper ions (*15*, *38*). This implies that a deprotonation of the hydroxy group occurs at some stage during the binding sequence, most likely catalyzed by a basic protein side chain residue as shown in Schemes 2 and 3. This idea is supported by kinetic data for tyrosinase and the X-ray crystal structure of the related enzyme catechol oxidase. The pH dependence of the lag phase for monophenolase activity of mushroom tyrosinase is associated with a pK_a of 6.8 in the met form

Scheme 3: Proposed Structural Reaction Mechanism for the Reaction of Oxytyrosinase with *o*-Diphenols[a]

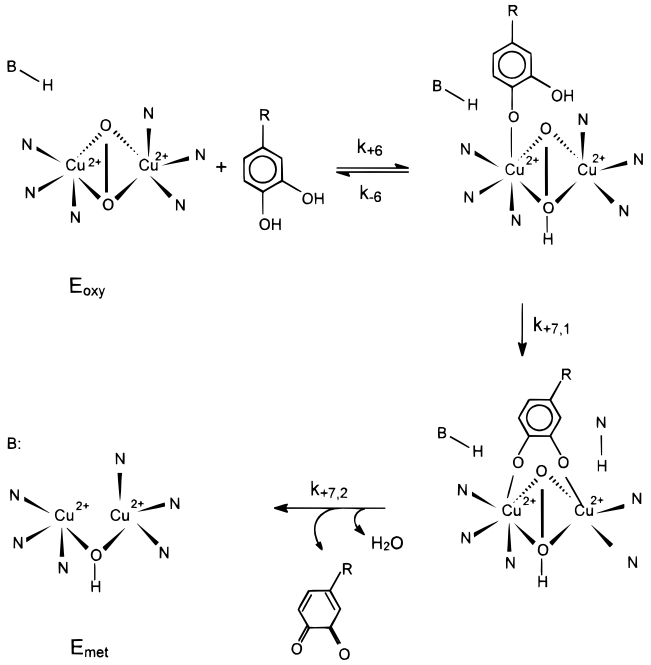

[a] This mechanism is based on the geometry and electronic structure of the oxyhemocyanin active site (*17*). The reaction designated k_{+7} has been separated into two substeps, $k_{+7,1}$ and $k_{+7,2}$, in order to discuss the rate-limiting step in the oxidation of *o*-diphenols by mushroom tyrosinase. Coordination of the *o*-diphenol to one copper of the binuclear site is accompanied by proton transfer to the bound peroxide. Bidentate coordination of the catechol substrate is accompanied by a second proton transfer. Electron transfer from the *o*-diphenol to the peroxide induces cleavage of the oxygen−oxygen bond to yield a water molecule and the quinone product while regenerating mettyrosinase. In this last step, the protein residue B acts as an acid, providing a proton for water release. As in Scheme 2, the value of $k_{+7,1}$ could be modulated by the steric and/or polar nature of the substrate.

(*36*, *39*). The protonated mettyrosinase has a lower affinity toward monophenol resulting in a lower concentration of the dead-end, inactive E_{met}-monophenol species. Thus, lowering the pH decreases the time required to reach a steady state, resulting in a shorter lag phase (*15*, *36*). In addition, the recently resolved crystal structure of sweet potato catechol oxidase (*37*) indicates that Glu-236 acts as a general acid/base catalyst for substrate binding. However, sequence data suggest that the equivalent residue in human and *Neurospora crassa* tyrosinase, where it is replaced by glutamine and leucine, respectively, has no equivalent functionality. The differences in the rates of binding of *o*-diphenols to the met and oxy forms of tyrosinase can be explained if the bound peroxide is the proton acceptor from the reducing substrate as suggested by Conrad et al. (*40*) and shown in Scheme 3. In support of this, extended Huckel theory calculations on a model of the oxyhemocyanin active center comprising six imidazoles, two coppers, and a dioxygen molecule gave molecular electrostatic potential maps predictive of protonation at bound dioxygen (*41*). Masuda et al. (*42*) have shown by X-crystallography that in a model L-tyrosyl-L-histidine−copper II complex, the protonated phenol—not the phenolate—form of tyrosine is coordinated to the Cu(II). They suggested that this type of coordination of substrates occurs at the active site of tyrosinase before facile proton transfer either to solvent or to an adjacent basic residue.

Scheme 4: Proposed Structural Changes Occurring When Oxygen Binds to Deoxytyrosinase[a]

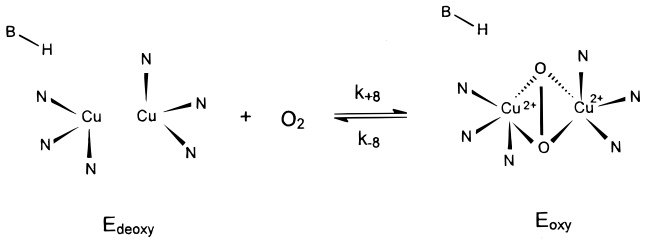

[a] The neutral environment provided by the protonated acid−base catalyst (BH) could favor the rapid binding of oxygen to deoxytyrosinase. In oxytyrosinase, the oxygen is proposed to bind in a side-on μ-η^2:η^2 peroxide fashion.

Binding of Oxygen to Tyrosinase. The proposed mechanism for the oxidation of *o*-diphenols (Scheme 1) and associated kinetic analysis explains the variation in $K_m^{O_2}$ with the nature of the *o*-diphenol observed by others (*21*−*23*). From the relationship between the catalytic constant (k_{cat}) and $K_m^{O_2}$ for the *o*-diphenols used in the present study, the value of the second-order rate constant for the reaction of oxygen with E_{deoxy} (k_{+8}) can be determined. This constant is, as expected, independent of the nature of the *o*-diphenol and has a value of 2.3×10^7 M^{-1} s^{-1}. This value is very similar to that reported for oxygen binding to hemocyanins [$(1.3 \times 10^6) - (5.7 \times 10^7)$ M^{-1} s^{-1} (*43*)] and to horse myoglobin (1.4×10^7 M^{-1} s^{-1}) and suggest that the access to the active site for oxygen is probably similar for tyrosinase and hemocyanins. The first-order rate constant for the dissociation of oxygen (k_{-8}) also has a high value of ca. 1.07×10^3 s^{-1}. These kinetic rate constants ensure the rapid binding of dioxygen to tyrosinase, thereby competing effectively with *o*-diphenol binding to deoxytyrosinase, which would otherwise lead to enzyme inhibition (*15*). The presence of a protonated base in deoxytyrosinase (Scheme 4) could facilitate oxygen binding and hinder the binding of the reducing substrate to this form of the enzyme. In the present study, the $K_D^{O_2}$ of tyrosinase ($K_D^{O_2} = 46.6$ μM) is shown to be of the same order as that of *Octopus vulgaris* hemocyanin ($K_D^{O_2} = 90$ μM) (*13*). Assuming similar structures and reactivities for the binuclear cupric peroxide species present in both proteins, the differences in activities observed toward *o*-diphenols (*11*) can be explained by severe steric constraints for the binding of phenolic substrates to hemocyanin (*13*).

Oxidation of o-Diphenols by Tyrosinase: Rate-Limiting Step. After binding, tyrosinase oxidizes *o*-diphenols to *o*-quinones. It has been proposed that the *o*-diphenol substrates are coordinated as phenolates to an axial position at a tetragonal cupric site, probably by displacement of a water molecule. The fact that *o*-diphenols but not *m*- or *p*-diphenols are oxidized by tyrosinase supports the idea of bridging, bidentate coordination of the diphenol between two coppers as shown in Schemes 2 and 3. However, bidentate coordination to a single copper is also a possibility (*20*). In either case, coordination of the second hydroxyl would involve displacement of a histidine residue from that copper (Scheme 2 and 3). Recently, a ^{1}H NMR study of *Streptomyces antibioticus* tyrosinase revealed that the hydrogen exchange behavior of one of the NH peaks from the six histidines bound to copper differs from that of the other five (*44*).

In our mechanism, two electrons would need to be transferred from the substrate to the binuclear copper II center

in mettyrosinase or to the bound peroxide in oxytyrosinase. The dependence of k_{cat} on the nature of the *o*-diphenol gives some insight into the nature of the rate-limiting step in the catalytic cycles of tyrosinase. It has been suggested that, for good reducing substrate activity, the *o*-diphenol should have increased electron density in the vicinity of the hydroxyl groups at position 3 and 4 (*22*). However, as can be observed in Table 1, substrates with similar redox potentials, such as catechol and L-dopa, are oxidized by tyrosinase at quite different rates. Thus, the highest k_{cat} is observed for substrates with no side chain (e.g., pyrogallol and catechol), followed by those with a hydrophobic side chain. The substrates most slowly oxidized are those with a polar side chain. The k_{cat} of tyrosinase is therefore modulated by the steric and polar characterics of the reducing substrate as was discussed by Solomon et al. (*20*). These results suggest that diphenol oxidation rates depend strongly on orientation and steric mobility within the hydrophobic pocket of tyrosinase.

APPENDIX

The coefficients G_i ($i = 1-4$) and g_i ($i = 1-4$) in the Kinetic analysis subsection of the Transient-Phase Kinetics section of the main paper have the following expressions:

$$G_1 = k_{-6} + k_{+7} + k_{-2} + k_{+3} + k_{-8} + k_{+8}[O_2]_0 + (k_{+2} + k_{+6})[D]_0$$

$$G_2 = (k_{-2} + k_{+3})(k_{-6} + k_{+7}) + k_{-8}(k_{-6} + k_{+7} + k_{-2} + k_{+3}) + k_{+8}(k_{-6} + k_{+7} + k_{-2} + k_{+3})[O_2]_0 + \{(k_{+3} + k_{+7})(k_{+2} + k_{+6}) + k_{+2}k_{-6} + k_{+6}k_{-2}\}[D]_0 + k_{+8}(k_{+2} + k_{+6})[D]_0[O_2]_0 + k_{+2}k_{+6}[D]_0^2$$

$$G_3 = k_{-8}(k_{-2} + k_{+3})(k_{-6} + k_{+7}) + k_{+8}(k_{-2} + k_{+3})(k_{-6} + k_{+7})[O_2]_0 + \{k_{+2}k_{+3}(k_{-6} + k_{+7}) + k_{+6}k_{+7}(k_{-2} + k_{+3}) + k_{-8}k_{+2}(k_{-6} + k_{+7} + k_{+3})\}[D]_0 + \{k_{+2}k_{+8}(k_{-6} + k_{+7} + k_{+3})k_{+6}k_{+8}(k_{-2} + k_{+3} + k_{+7})\}[D]_0 [O_2]_0 + k_{+2}k_{+6}(k_{+3} + k_{+7})[D]_0^2 + k_{+2}k_{+6}k_{+8}[D]_0^2[O_2]0$$

$$G_4 = k_{+2}k_{+3}k_{-8}(k_{-6} + k_{+7})[D]_0 + k_{+8}\{k_{+2}k_{+3}(k_{-6} + k_{+7}) + k_{+6}k_{+7}(k_{-2} + k_{+3})\}[D]_0[O_2]_0 + k_{+2}k_{+3}k_{+6}k_{+7}[D]_{02} + k_{+2}k_{+6}k_{+8}(k_{+3} + k_{+7})[D]_0^2[O_2]_0$$

$$g_1 = k_{-6} + k_{+7} + k_{-2} + k_{+3} + k_{+8}[O_2]_0 + k_{+2}[D]_0$$

$$g_2 = (k_{-2} + k_{+3})(k_{-6} + k_{+7}) + k_{+8}(k_{-6} + k_{+7} + k_{-2} + k_{+3})[O_2]_0 + k_{+2}(k_{-6} + k_{+7} + k_{+3})[D]_0 + k_{+2}k_{+8}[D]_0[O_2]_0$$

$$g_3 = k_{+8}(k_{-6} + k_{+7})(k_{-2} + k_{+3})[O_2]_0 + k_{+2}k_{+3}(k_{-6} + k_{+7})[D]_0 + k_{+2}k_{+8}(k_{-6} + k_{+7} + k_{+3})[D]_0[O_2]_0$$

$$g_4 = k_{+2}k_{+3}k_{+8}(k_{-6} + k_{+7})[D]_0[O_2]_0$$

REFERENCES

1. Prota, G. (1988) *Med. Res. Rev. 8*, 525−556.
2. Zawistowski, J., Biliaderis, C. G., and Eskin, N. A. M. (1991) in *Oxidative Enzymes in Foods* (Robinson, D. S., Eskin, N. A. M., Eds.) pp 217−273, Elsevier Science, London.
3. Robb, D. A. (1984) in *Copper Proteins and Copper Enzymes* (Lontie, R., Ed.) pp 207−241, CRC Press, Boca Raton, FL.
4. Mason, H. S. (1956) *Nature 177*, 79−81.
5. Lerch, K. (1981) in *Metal Ions in Biological Systems.* (Sigel, H., Ed.) pp 143−186, Marcel Dekker, New York.
6. Sánchez-Ferrer, A., Rodríguez-López, J. N., García-Cánovas, F., and García-Carmona, F. (1994) *Biochim. Biophys. Acta 1247*, 1−11.
7. García-Cánovas, F., García-Carmona, F., Vera-Sánchez, J., Iborra, J. L., and Lozano, J. A. (1982) *J. Biol. Chem. 257*, 8738−8744.
8. Rodríguez-López, J. N., Tudela, J., Varón, R., García-Carmona, F., and García-Cánovas, F. (1992) *J. Biol. Chem. 267*, 3801−3810.
9. Yong, G., Leone, O., and Strothkamp, K. G. (1990) *Biochemistry 29*, 9684−9690.
10. Deinum, J., Lerch, K., and Reinhammar, B. (1976) *FEBS Lett. 69*, 161−164.
11. Himmelwright, R. S., Eickman, N. C., LuBien, C. D., Lerch, K., and Solomon, E. I. (1980) *J. Am. Chem. Soc. 102*, 7339−7344.
12. Messerschmidt, A., and Huber, R. (1990) *Eur. J. Biochem. 187*, 341−352.
13. Salvato, B., Santamaria, M., Beltramini, M., Alzuet, G., and Casella, L. (1998) *Biochemistry 37*, 14065−14077.
14. Jolley, R. L., Jr., Evans, L. H., Makino, N., and Mason, H. S. (1974) *J. Biol. Chem. 249*, 335−345.
15. Wilcox, D. E., Porras, A. G., Hwang, Y. T., Lerch, K., Winkler, M. E., and Solomon, E. I. (1985) *J. Am. Chem. Soc. 107*, 4015−4027.
16. Solomon, E. I. (1981) in *Copper Proteins* (Spiro, T. G., Ed.) pp 41−108, Wiley-Interscience, New York.
17. Magnus, K., and Ton-That, H. (1992) *J. Inorg. Biochem. 47*, 20.
18. Kitajima, N., Fujisawa, K., Moro-oka, Y., and Toriumi, K. (1989) *J. Am. Chem. Soc. 111*, 8975−8976.
19. Baldwin, M. J., Root, D. E., Pate, J. E., Fujisawa, K., Kitajima, N., and Solomon, E. I. (1992) *J. Am. Chem. Soc. 114*, 10421−10431.
20. Solomon, E. I., Sundaram, U. M., and Machonkin, T. E. (1996) *Chem. Rev. 96*, 2563−2605.
21. Ingraham, L. L. (1957) *J. Am. Chem. Soc. 79*, 666−669.
22. Duckworth, H. W., and Coleman, J. E. (1970) *J. Biol. Chem. 245*, 1613−1625.
23. Janovitz-Klapp, A. H., Richard, F. C., Goupy, P. M., and Nicolas, J. J. (1990) *J. Agric. Food Chem. 38*, 1437−1441.
24. Rodríguez-López, J. N., Ros, J. R., Varón, R., and García-Cánovas, F. (1993) *Biochem J. 293*, 859−866.
25. Kertesz, D., Brunori, M., Zito, R., and Antonini, E. (1971) *Biochim. Biophys. Acta 250*, 306−310.
26. Makino, N., and Mason, H. S. (1973) *J. Biol. Chem. 248*, 5731−5735.
27. Goodwin, D. C., Yamazaki, I., Aust, S. D., and Grover, T. A. (1995) *Anal. Biochem. 231*, 333−338.
28. Ros, J. R., Rodríguez-López, J. N., and García-Cánovas, F. (1993) *Biochem. J. 295*, 309−312.
29. Bradford, M. M. (1976) *Anal. Biochem. 72*, 248−256.
30. Rodríguez-López, J. N., Ros, J. R., Varón, R., and García-Cánovas, F. (1992) *Anal. Biochem. 202*, 356−360.
31. Jackman, M. P., Huber, M., Hajnal, A., and Lerch, K. (1992) *Biochem J. 282*, 915−918.
32. Cornish-Bowden, A. (1979) in *Fundamentals of Enzyme Kinetics*, pp 34−37, Butterworth and Co., London.
33. Marquardt, D. W. (1963) *J. Soc. Ind. Appl. Math. 11*, 431−441.
34. Jandel Scientific (1994) *Sigma Plot 2.01 for Windows*, Jandel Scientific, Corte Madera, CA.
35. García-Sevilla, F., Garrido del Solo, C., Duggleby, R. G., García-Cánovas, F., Peyro García, R., and Varón, R. (2000) *BioSystems 54*, 151−164.
36. Ros, J. R., Rodríguez-López, J. N., and García-Cánovas, F. (1994) *Biochim. Biophys. Acta 1204*, 33−42.
37. Klabunde, T., Eicken, C., Sacchettini, J. C., and Krebs, B. (1998) *Nature Struct. Biol. 5*, 1084−1090.
38. Toussaint, O., and Lerch, K. (1987) *Biochemistry 26*, 8567−8571.

39. Espín, J. C., Varón, R., Tudela, J., and García-Cánovas, F. (1997) *Biochem. Mol. Biol. Int. 41*, 1265−1276.
40. Conrad, J. S., Dawso, S. R., Hubbard, E. R., Meyers, T. E., and Strothkamp, K. G. (1994) *Biochemistry 33*, 5739−5744.
41. Eisenstein, O., Giessner-Prettre, C., Maddaluno, J., Stussi, D., and Weber, J. (1992) *Arch. Biochem. Biophys. 296*, 247−255.
42. Masuda, H., Odami, A., and Yamauchi, O. (1989) *Inorg. Chem. 28*, 624−625.
43. Jameson, G. B., and Ibers, J. A. (1994) in *Bioinorganic Chemistry* (Bertini, I., Gray, H. B., Lippard, S. J., and Valentine, J. S., Eds.) pp 167−252, University Science Books, Mill Valley, CA.
44. Bubacco, L., Salgado, J., Tepper, A. W. J. W., Vijgenboom, E., and Canters, G. W. (1999) *FEBS Lett 442*, 215−220.
45. Solomon, E. I., and Lowery, M. D. (1993) *Science 259*, 1575−1581.

BI000539+